Inhibition of Ice Recrystallization by Nanotube-Forming Cyclic Peptides

Romà Surís-Valls, Tim P. Hogervorst, Sandra M. C. Schoenmakers, Marco M. R. M. Hendrix, Lech Milroy, and Ilja K. Voets*

ACCESS | Metrics & More | Article Recommendations | Supporting Information

ABSTRACT: While most native ice-binding proteins are rigid, artificial (macro)molecular ice-binders are usually flexible. Realizing a regular array with precisely positioned ice-binding motifs on synthetic proteins, (macro)molecular ice-binders are thus challenging. Here, we exploit the predictable assembly of cyclic peptides into nanotubes as a starting point to prepare large, rigid ice-binders bearing an ice-binding site that is found in hyperactive ice-binding proteins in insects. First, we designed, synthesized, and purified cyclic octapeptide Lys2CP8 bearing a TaT motif to promote ice binding and investigated their solution assembly and activity using

circular dichroism (CD) spectroscopy, Fourier-transform infrared (FTIR) spectroscopy, light scattering (LS), cryogenic transmission electron microscopy (cryo-TEM), and ice recrystallization inhibition (IRI) assays. The cyclic peptide Lys2CP8 was synthesized in good yield using Fmoc chemistry and purified by reversed-phase HPLC. Upon dissolution in aqueous solutions, Lys2CP8 was observed to assemble in a pH- and concentration-dependent manner into objects with nanoscopic dimensions. LS revealed the presence of small and large aggregates at pH 3 and 11, held together through a network of intermolecular antiparallel β-sheets as determined by FTIR and CD spectroscopy. Cryo-TEM revealed the presence of one-dimensional objects at pH 3 and 11. These are mostly well-dispersed at pH 3 but appear to bundle at pH 11. Interestingly, the pH-dependent self-assembly behavior translates into a marked pH dependence of IRI activity. Lys2CP8 is IRI-active at pH 3 while inactive at pH 11 hypothetically because the ice-binding sites are inaccessible at pH 11 due to bundling.
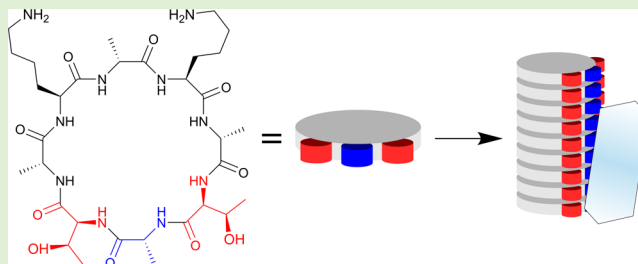
INTRODUCTION

Ice-binding proteins (IBPs) emerged as pivotal macromolecular cryoprotectants in natural response strategies to render cold, ice-laden environments habitable.[1,2] By controlling ice formation and growth through various mechanisms, IBPs in fish, insects, algae, bacteria, and plants protect against freezing-induced injuries.[1,2] Antifreeze proteins in fish create a so-called thermal hysteresis gap to defer explosive growth of macroscopic ice crystals to lower temperatures and maintain blood circulation.[3] Microalgae and bacteria utilize IBPs to create and adhere to an environmental niche rich in nutrients, light, and oxygen.[4] Bacterial ice-nucleating proteins promote nucleation[5] and plant IBPs inhibit ice recrystallization.[6] The key to these diverse coping mechanisms of freezing point depression (thermal hysteresis, TH),[3,7] ice recrystallization inhibition (IRI),[6,8] ice nucleation (IN),[5] and ice-adhesion[9] is the ability of IBPs to adhere to (specific faces of) ice crystals.[1,2,7]

Inspired by native IBPs, a broad spectrum of artificial ice-binders has been developed aiming to create novel materials with the cryoprotective power of IBPs, which are amenable to deployment in non-natural and complex environments for deicing, anti-icing, ice-templating, and cryopreservation.[2] The

synthesis and performance of IRI-active compounds has been a particularly active field in recent years, yielding small molecular,[10] peptidic,[11−13] and polymeric[14] IBP analogues with low-to-moderate IRI activity and little-to-no thermal hysteresis nor ice nucleation activity. These artificial, (macro)-molecular cryoprotectants tend to be flexible, moderately soluble, and prone to aggregation, especially if limited (charged) hydrophilic functionalities are incorporated to improve solubility.[15] This may mask the ice-binding site or interfere with the facial amphiphilicity required for IRI.[14] By contrast, many natural IBPs comprise a rigid, native fold with a flat and hydrophobic, often threonine-rich, ice-binding site (IBS) opposed to or flanked by hydrophilic regions for solubility.[16]

An appealing class of materials ideally suited to produce well-defined, rigid structures with a customizable surface are
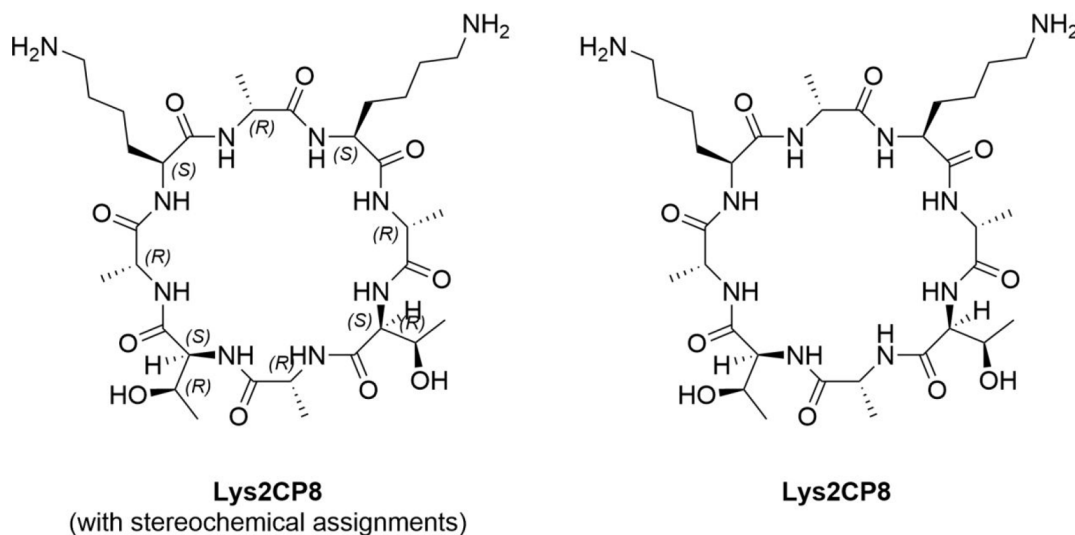
Scheme 1. Chemical Structure of D-/L-Alternating Cyclic Octapeptide Equipped with Ice-Binding Moieties[a]

Lys2CP8
(with stereochemical assignments)

Lys2CP8

[a]Lys2CP8, with alternating D-/L-stereochemistry and the TaT ice-binding motif were prepared comprising four D-alanine residues bracketed by two L-threonine and two L-lysine residues, that is, *cyclo*-(KaKaTaTa) or Lys2CP8. The structure is displayed in the neutral state. At sufficiently low pH values (pKa_{Lys} ∼ 10.5), Lys2CP8 becomes positively charged.

self-assembling (cyclic) peptides[17−19] and their derivatives, such as peptide amphiphiles[20] and peptoids.[21,22] Of particular interest are those for which the relation between the molecular structure and supramolecular architecture is predictable. Such is the case for peptide nanotubes of cyclic peptides (CP), for example.[23,24] This offers the exciting possibility to adapt the molecular design of previously reported nanotube-forming peptides to surface-display known ice-binding sites on nanotubes of a few nanometers wide and a few tens or hundreds of nanometers long.

Inspired by the work of Ghadiri et al. on nanotube-forming cyclic peptides,[25] we designed and synthesized an alternating L- and D-cyclic octapeptide, here forth referred to as Lys2CP8 (Scheme 1), as a potential, self-assembling ice-binding CP. Besides the classical alternating sequence of L- and D-amino acids which is well-known to induce stacking of the CP into antiparallel β-sheets,[26,27] the structure of our Lys2CP8 included a TaT sequence (T denoting L-threonine, a denoting D-alanine), as found in, for example, hyperactive insect antifreeze proteins, with the intention of creating an ice binding site in the stacked CP, and two lysines to improve aqueous solubility and introduce potential pH responsiveness. Results from light scattering studies on Lys2CP8 demonstrated aggregation in aqueous solutions, induced presumably by antiparallel β-sheet formation. Cryo-TEM imaging revealed that Lys2CP8 formed stacks with high aspect ratios, which bundle in aqueous alkaline solutions (pH 11). IRRINA (Ice Recrystallization Rate Inhibition Analysis) assays of IRI activity[8] at different pH values showed that Lys2CP8 inhibits ice recrystallization in a pH-dependent manner. Interestingly, while inactive at pH 11, Lys2CP8 inhibited ice recrystallization at pH 3 in a concentration-dependent manner. We propose that this interesting pH- and concentration-dependent IRI activity is related to nanotube formation and bundling. The latter is most prevalent at pH 11 and hypothetically masks the ice-binding sites on the surface of the nanotubes so as to render the superstructures inactive at pH 11.

■ EXPERIMENTAL SECTION

Materials. All Fmoc-protected amino acids and coupling reagents for peptide synthesis were purchased from Novabiochem and were used as received. The resins used for solid phase peptide synthesis (SPPS) were purchased from IrisBiotech. Solvents for peptide synthesis were purchased from Biosolve. Deuterated solvents were obtained from Cambridge Isotope Laboratories. Dry solvents were obtained using a MBRAUN Solvent Purification System (MB-SPS).

Solid-Phase Peptide Synthesis of Lys2CP8. *Synthesis of Crude, Partially Protected, Linear H-aK(tBoc)aT(tBu)aT(tBu)aK-(tBoc)−OH Peptide (Figure S1).* H-L-Lys(Boc)-2-chlorotrityl resin (400 μmol) was weighed into a fritted polypropylene syringe and preswollen in DMF (12 mL) for 30 min at room temperature agitating on an orbital shaker (500 rpm). The solvent was drained and treated with a preprepared solution of Fmoc-D-Ala-OH (2.5 equiv), HBTU (2.5 equiv), and DIPEA (8 equiv) in anhydrous DMF and agitated at room temperature for 3 h. The solvents were drained and the resin washed sequentially with DMF (5 × 8 mL), CH_2Cl_2 (5 × 8 mL) and DMF (5 × 8 mL). The resin was then treated with 20% piperidine in DMF (8 mL, 3 min, ×3) to cleave the Fmoc group and subsequently washed with DMF (5 × 8 mL), CH_2Cl_2 (5 × 8 mL), and DMF (5 × 8 mL). The above sequence of steps was repeated in a cyclical manner using the requisite Fmoc-protected amino acid building block until completion of the linear amino acid sequence (Figure S1). The resin was then thoroughly washed (×5) with CH_2Cl_2 and then preswollen in 15 mL of CH_2Cl_2 for 30 min at room temperature agitating on an orbital shaker (500 rpm), drained, and then treated with a solution of 1,1,1,3,3,3-hexafluoroisopropanol (HFIP): CH_2Cl_2 (1:4 v/v, 8 mL, 10 min, ×3). After collecting the solvents, the resin was washed with CH_2Cl_2 (3 × 8 mL) and the solvents combined and concentrated under reduced pressure by rotary evaporation. Subsequent oil-pump high vacuum drying afforded a crude residue, which was dissolved in deionized water and lyophilized to afforded the crude, partially protected, linear peptide.

Synthesis of Lys2CP8 (Figure S1). Thirty milligrams (∼28 μmol) of the crude, partially protected, linear peptide was weighed in a round-bottom neck flask fitted with a septum. The flask was flushed with argon and the crude peptide dissolved in 22.5 mL of dry DMF. A solution containing 5 equiv (23 mg, 140 μmol) of 4-(4,6-dimethoxy-1,3,5-triazin-2-yl)-4-methylmorpholinium tetrafluoroborate (DMTMM·BF₄) was prepared in dry DMF, flushed with argon, and then added to the peptide solution until a final volume of 30 mL was

obtained. The reaction mixture was then magnetically stirred (500 rpm) overnight at room temperature under a positive argon pressure. The DMF was removed by rotary evaporation (5 mbar, 1 h) and the resultant residue dissolved in deionized water and lyophilized. The crude, protected Lys2CP8 was then purified by preparative HPLC and the pure, protected Lys2CP8 was characterized by MALDI-MS (Figure S2e). The protected Lys2CP8 peptide was then treated for 3 h with TFA/TIS/H_2O (95/2.5/2.5, v/v), the solvents were evaporated under a gentle stream of argon, and Lys2CP8 was isolated by precipitation (ice-cold diethyl ether) and lyophilization (Milli-Q water). The final Lys2CP8 peptide was characterized by MS and ^1H NMR. Please refer to the SI for more information.

Synthesis of Lys2LP8 (Figure S1). The synthesis of linear control peptide Lys2LP8 is described in the SI.

Sample Preparation. The pH of 100 mM NaCl aqueous solutions was adapted by the addition of concentrated HCl or NaOH solutions. The desired amount of peptide powder was weighted into a suitable container, after which the 100 mM NaCl aqueous solution was added to reach the desired concentration. All samples appeared to dissolve well upon ocular inspection without exception. All samples were prepared in 100 mM NaCl except for circular dichroism spectroscopy, for which 10 mM NaH_2PO_4 at pH 7.2 was used instead to ensure sufficiently low high-tension values. All samples were allowed to equilibrate overnight before measurements were performed. Concentration series were prepared upon serial dilution of a suitable stock solution in 100 mM NaCl at pH 3 and pH 11.

METHODS

Dynamic and Static Light Scattering (DLS/SLS). Light scattering measurements were performed on an ALV/CGS-3 MD-4 goniometer system, equipped with a 50 mW Nd:YAG laser operating at a wavelength λ of 532 nm. A refractive index matching bath of filtered decalin surrounded the cylindrical scattering cell and the temperature was regulated using a Lauda RM6-S refrigerated circulating water bath to remain fixed at 20.0 °C ± 0.1. Light scattering experiments were performed on salted aqueous solutions at a fixed 100 mM NaCl concentration to suppress structuring due to electrostatic interactions which could hamper data analysis. Static light scattering (SLS): The total averaged scattered intensity was recorded five times at a fixed angle of 90°. Dynamic light scattering (DLS): The second-order correlation function, $g_2(t)$, was recorded five times at a fixed angle of 90°. The five runs were averaged for each sample and analyzed via the inverse Laplace transformation according to the CONTIN algorithm implemented in the AfterALV software package to compute an apparent hydrodynamic radius, R_h, via the Stokes–Einstein equation and to generate equal area representations of the apparent size distributions.

Circular Dichroism Spectroscopy. Circular dichroism measurements were performed on a Jasco J-815 spectropolarimeter in the wavelength range 190–260 nm at a scanning speed of 50 nm min^{-1} with 2 s accumulation, 1 nm bandwidth, and a data pitch of 0.5 nm. Samples were measured in a 0.1 cm quartz cuvette at a fixed Lys2CP8 concentration of 0.012 wt % (62 μM) prepared by direct dissolution of 0.1 mg of dry peptide powder into a 10 mM NaH_2PO_4 buffer (pH 7.2). This sample composition was selected to maximize signal-to-noise ratio and ensure HT values remained below 650 V. CD traces were obtained upon averaging at least three measurements followed by background subtraction. Data is plotted using a three-point moving average. To elucidate the details of structural reorganization, secondary structure deconvolution was performed on the online Dichroweb server using the CDSSTR algorithm and associated reference set 4.[28,29] All outputs satisfied the condition of NRMSD < 0.025.

Cryogenic Transmission Electron Microscopy. Peptide nanotube samples were prepared at a concentration of 5 mM by dissolving the purified cyclic Lys2CP8 in 100 mM NaCl solutions at a pH 3 or pH 11. All of the samples appeared to dissolve well upon ocular inspection. Afterward, the samples were allowed to equilibrate overnight before the measurements were performed. Vitrified films were prepared in a "Vitrobot" instrument (FEI Vitrobot Mark IV, FEI Company) at 22 °C and at a relative humidity of 100%. In the preparation chamber of the Vitrobot, 3 μL samples were applied on Quantifoil grids (R 2/2, Quantifoil Micro Tools GmbH), which were surface plasma treated just prior to use (Cressington 208 carbon coater operating at 5 mA for 40 s). Excess sample was removed by blotting using filter paper for 4 s with a blotting force of −1, and the thin film thus formed was plunged (acceleration about 3 g) into liquid ethane just above its freezing point. Vitrified films were transferred into the vacuum of a CryoTITAN equipped with a field emission gun that was operated at 300 kV, a postcolumn Gatan energy filter, and a 2048 × 2048 Gatan CCD camera. Vitrified films were observed in the CryoTITAN microscope at temperatures below −170 °C. Micrographs were taken at low dose conditions, starting at a magnification of 6500 with a defocus of −40 μm, and at a magnification of 24 000 with a defocus of −10 μm.

Ice Recrystallization Inhibition Assay. IRRINA (Ice Recrystallization Rate Inhibition Analysis) assays of ice recrystallization inhibition were performed at peptide concentrations between 0.1 and 15 mM peptide in a 30 wt % sucrose solution. The sucrose solution was prepared by dissolution of a preweighted amount of sucrose to yield 30 wt % of sucrose in a solution of 100 mM NaCl at pH3 or 11. The peptide solutions were prepared upon serial dissolution of a peptide stock with the corresponding sucrose stock. All of the samples appeared to dissolve well upon ocular inspection, and no visual aggregates were observed with the exception of the Lys2CP8 sample at a 15 mM when dissolved in 100 mM NaCl at pH 11. Afterward, the samples were allowed to equilibrate overnight before the measurements were performed. Samples of 2 μL were sandwiched between two precleaned cover slides, which were rapidly frozen (20 °C min^{-1}) to −40 °C in a Linkam LTS420 stage attached to a Nikon ECLIPSE Ci-Pol Optical Microscope. The samples were annealed for 90 min at a set annealing temperature of −7 °C, corresponding to a sample annealing temperature of −7 ± 1 °C. Microphotographs were taken every 2 min using a Lumera3 CCD camera to follow the ice growth over time. All samples showed well-defined grain boundaries and frozen fractions lower than 0.3, which made them suitable for the study of migratory recrystallization and minimized ice crystal accretion.

Fourier-Transform Infrared Spectroscopy. Fourier-transform infrared spectroscopy measurements were performed on a Spectrum TWO LiTa FT-IR Spectrometer (PerkinElmer, Llantrisan, U.K.) in the wavenumber range 1000 and 3250 cm^{-1} and a data pitch of 2 cm^{-1}. Solid-state samples were prepared by grinding Lys2CP8 powder with KBr in a 100:1 (w/w) ratio. After homogenizing the sample, the ground mixture was pressed to obtain a 5 mm KBr-sample pellet that was transferred to the sampling chamber with tweezers. During the experiment, N_2 (g) was constantly flushed to the solid sample to remove moisture from the environment. FTIR traces were obtained upon averaging eight accumulations followed by background subtraction. Plotted data corresponds to means of eight accumulations.

RESULTS AND DISCUSSION

Design of Lys2CP8 Bearing Ice Binding Moieties. Inspired by the work of Ghadiri et al. on self-assembling cyclic peptides (CPs),[25] we selected an alternating L- and D-octapeptide as scaffold to create a CP with the potential to self-assemble into nanotubes with aligned ice-binding moieties on their exterior. The alternating stereochemistry proposed by Ghadiri et al. promotes the formation of dihedral β-type angles to form a closed ring structure that stacks into nanotubes through hydrogen bonding.[25] The scaffold also ensures that the amide and carboxyl groups are aligned parallel to the long axis of the cylinders, while the side chains of the amino acids are axially projected. Such octapeptide sequences thus offer an appealing platform to prepare cylindrical superstructures with surfaces tailored to facilitate, for example, hierarchical
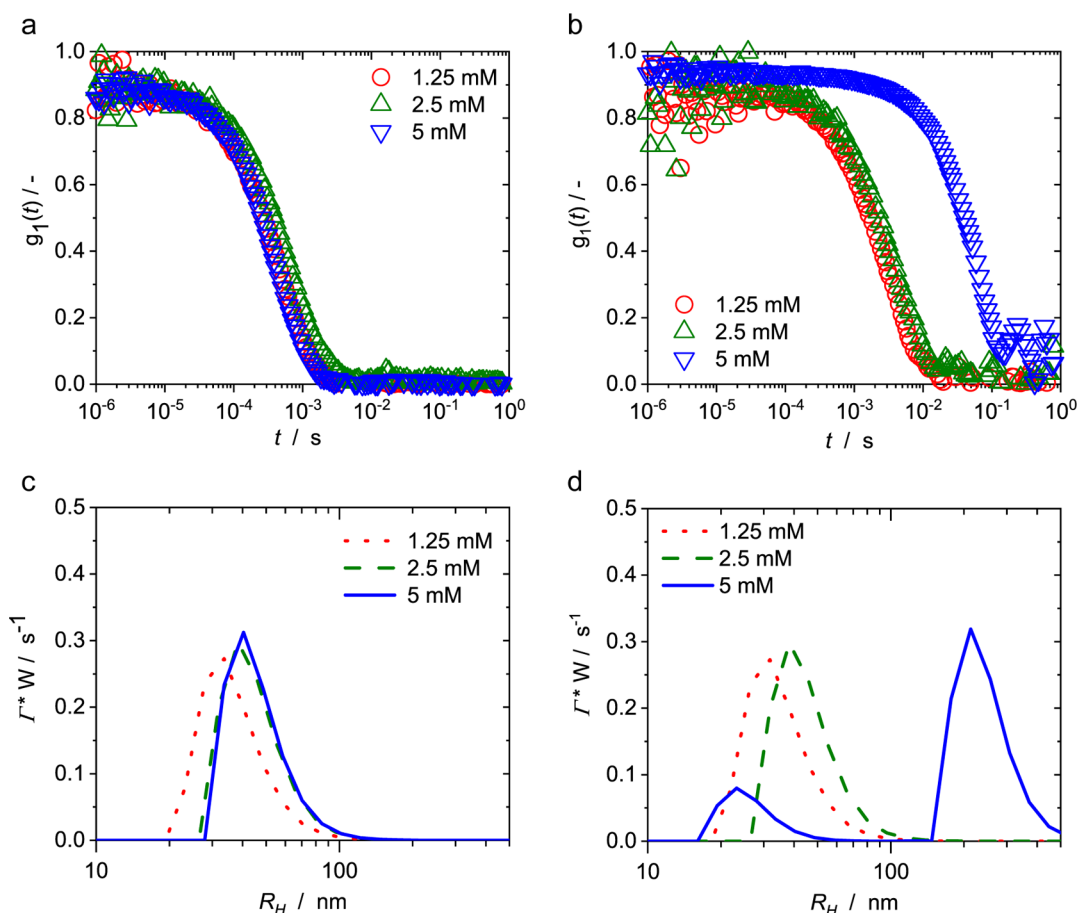
Figure 1. Dynamic light scattering. (a, b) First order autocorrelation functions and (c,d) corresponding size distributions in equal area representations of 1.25, 2.5, and 5 mM Lys2CP8 in 100 mM NaCl at (a,c) pH 3 and (b,d) pH 11.

aggregation[30] or interact with solid surfaces[30,31] and membranes of living cells.[32] Here, we install the TaT ice-binding motif (T denoting L-threonine, a denoting D-alanine) to prime the self-assembling CP to bind ice and thereby create an example of a potential cyclic ice-binding peptides (cIBPs, Scheme 1). Regular TXT arrays, comprising threonines (T) and any small amino acid (X), serve as ice-binding sites in β-helical-rich insect antifreeze proteins (AFPs), for example, from *Tenebrio molitor* (*Tm*AFP) and spruce budworm (*sbw*AFP).[16,33,34] If the cIBPs successfully assemble into nanotubes with rigid and aligned TaT regions, these synthetic architectures may likewise interact favorably with ice. To explore this possibility, we decided to prepare Lys2CP8, with a balanced amphiphilicity and pH-dependent ionization through incorporation of four D-alanines, two L-threonines, and two L-lysines (Lys2CP8) (Scheme 1). Interestingly, this design may offer a convenient handle to tune self-assembly and activity, since the pH-dependent degree of ionization of the incorporated Lys may impact peptide solubility, assembly, and concomitantly ice binding. We anticipate that stacking is strongly promoted at low degrees of ionization, corresponding to basic conditions for Lys2CP8 ($pK_{aLys} \sim 10.5$). Molecular dynamics simulations by Brotzakis et al. on Lys2CP8 nanotubes revealed the potential of this design.[35] In their work, the putative ice-binding sites aligned resulting in a flat and hydrophobic region on the nanotubes with intra- and intermolecular C^{α}-C^{α} distances for the threonines of 7.04 and 4.88 Å, respectively.[35] Both features are important as they are

likely related to ice-binding activity. Ice-binding sites (IBS) on native AFPs are typically flat and rather hydrophobic.[1,2] Moreover, IBS C^{α}-C^{α} distances typically match oxygen spacings on hexagonal ice. The modeled C^{α}−C^{α} distances are in close agreement with the corresponding distances in *Tm*AFP of 7.35 and 4.50 Å, respectively, and the oxygen spacing along the *c*- and *a*-axis of hexagonal ice (7.4 and 4.5 Å, respectively).[16] On average, more than one water molecule was observed to engage in hydrogen bonding with the hydroxyl groups of the threonine residues in the flat TaT region,[35] which holds promise for the intended interaction with ice.

Synthesis, Purification, and Characterization of TaT Bearing Lys2CP8. For the synthesis of Lys2CP8, we adapted the solid-phase synthesis approach to cyclic, alternating L- and D-octapeptides reported by Ghadiri and co-workers.[25] Instead of a Boc/Benzyl-based strategy, during which peptide cyclization is performed on-resin, we chose to follow a milder Fmoc-based strategy[36] in which the partially protected linear octapeptide is cleaved from the resin and subsequently cyclized in solution (Figure S1). *N*-[(1*H*-Benzotriazol-1-yl)-(dimethylamino)methylene]-*N*-methylmethanaminium hexa-fluorophosphate *N*-oxide (HBTU)[37] was used as the peptide coupling agent, combined with a 3 h incubation time per coupling step, to deliver the crude, partially protected linear peptide in an unoptimized 83% yield after resin cleavage with HFIP/CH$_2$Cl$_2$ (1:4, v/v) and lyophilization from deionized water. The linear peptide was characterized by LC-MS (Figure S2ab). The same synthesis was also demonstrated using the

analogous O-(1H-6-chlorobenzotriazol-1-yl)-1,1,3,3-tetrame-thyluronium hexafluorophosphate (HCTU)[38] instead of HBTU, combined with a significantly reduced reaction time (10 min), to yield the same peptide albeit in a slightly lower 75% yield. At the key cyclization step (Figure S1), initial attempts to close the ring using benzotriazole-1-yl-oxy-tris-pyrrolidino-phosphonium hexafluorophosphate (PyBOP)[39] failed. Ultimately, cyclization was achieved with DMTMM·BF$_4$ in an unoptimized 89% conversion according to LC-MS. DMTMM·BF$_4$[40] carries the advantage of not requiring additional base, which disfavors diastereomer formation through product isomerization during the cyclization step. The protected Lys2CP8 was purified by preparative LC-MS and characterized by LC-MS (Figure S2c,d) and MALDI-MS (Figure S2e). Deprotection of the lysine and threonine protecting groups using TFA/TIS/H$_2$O (95.0/2.5/2.5, v/v), followed by precipitation (ice-cold ether) and lyophilization (Milli-Q water), delivered Lys2CP8 in an unoptimized 82% yield. The Lys2CP8 was characterized by MS (Figure S2f) and ^{1}H NMR spectroscopy (Figure S3).

pH-Dependent Self-Assembly. To establish the conditions conducive to self-assembly of the cyclic octapeptides, light scattering experiments were performed at 1.25 mM, 2.5 mM, and 5 mM Lys2CP8 at two distinct pH values, one below (pH 3) and one above (pH 11) the pK_{aLys} ∼ 10.5 of the lysine side chains. The peptides are thus maximally ionized at pH 3 and conversely, near-neutral at pH 11. A fixed background salt concentration of 100 mM NaCl was used to suppress structuring effects which hamper particle sizing by light scattering. Importantly, the scattering intensity of the peptide solutions far exceeded the scattering intensity of the background solvent without any peptide, irrespective of pH and peptide concentration. Apparently, the peptides self-assemble into superstructures under all tested conditions.

To determine the size of the aggregates and shed light on the size distributions, dynamic light scattering (DLS) experiments were performed (Figure 1). At pH 3, the first order autocorrelation functions, $g_1(t)$, are virtually identical, regardless of peptide concentration, while they are clearly concentration-dependent at pH 11, shifting toward longer relaxation times upon increasing concentration (Figure 1a,b). The corresponding size distributions (Figure 1c,d) are virtually monomodal irrespective of pH except for the 5 mM sample at pH 11. The corresponding apparent hydrodynamic radii, R_h range from 57 to 565 nm, which is far larger than the dimensions of the cyclic peptide monomer (∼1 nm), confirming association under all tested conditions. The dimensions of the nanotubes are smaller at pH 3 than at pH 11 with the difference being small at 1.25 mM and much more pronounced at 5 mM. Clearly, the higher net charge makes the peptide more soluble and disfavors aggregation. Nonetheless, the driving forces for aggregation outweigh the screened electrostatic repulsion between Lys2CP8 monomers at pH 3, such that the cyclic peptide also aggregates under acidic conditions. The increase in R_h upon increasing peptide concentration under basic conditions, suggests that the cyclic peptide assembles into larger aggregates at higher concentrations. Assuming that Lys2CP8 assembles into peptide nanotubes as designed, the DLS results indicate that the Lys2CP8 nanotubes increase in length, or tend to bundle, as the peptide concentration is raised from 1.25 to 5 mM at pH 11.

Antiparallel $β$-Sheets in the Peptide Aggregates. To elucidate the nature of the intermolecular hydrogen bonding interactions and concomitant secondary structural elements involved in the association of the cyclic peptides, we turned to circular dichroism (CD) spectroscopy (Figure 2). The CD
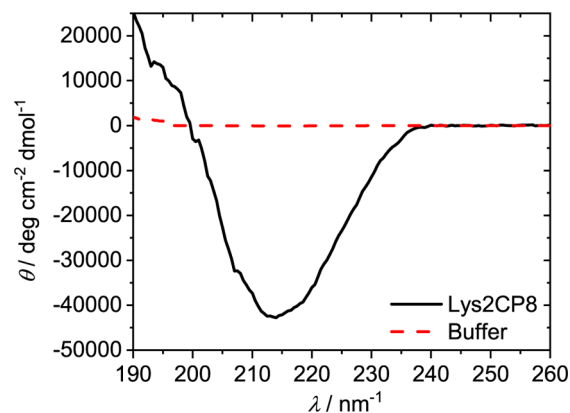

Figure 2. Circular dichroism spectroscopy. CD spectra of (solid black) a 62 $μ$M Lys2CP8 solution in 10 mM NaH$_2$PO$_4$ (pH 7.2) and (dashed red) the negative control comprising a 10 mM NaH$_2$PO$_4$ (pH 7.2) solution without any peptide.

spectrum of a 62 $μ$M Lys2CP8 solution in 10 mM NaH$_2$PO$_4$ reveals two clear features: an apparent maximum around a wavelength $λ$ ∼ 190 nm (which is the lowest accessible wavelength) and a pronounced minimum at a wavelength $λ$ ∼ 213 nm. These are inconsistent with predominantly $α$-helical or disordered structures, which would give rise to two minima ($α$-helices) and a minimum near $λ$ ∼ 195 nm (disordered). The spectrum is in line with those recorded for $β$-helical proteins, which exhibit a single minimum around 215 nm and a maximum at $λ$ ∼ 195 nm. We propose that these are likely antiparallel $β$-sheet structures, since these configurations have been reported previously by others for nanotubes comprising cyclic peptides with alternating L- and D-amino acids.[25,41]

Having established that the aggregates are $β$-sheet rich, we performed Fourier-transform infrared (FTIR) experiments to shed further light on their secondary structure. In line with the CD results, Lys2CP8 in solid-state displayed a number of bands at frequencies characteristic for $β$-sheet structures[42,43] (Figure 3a), such as the C=O amide-I band at 1630 cm^{-1}. This is typically attributed to the formation of antiparallel $β$-sheets between peptide backbones. Other pronounced bands include a C=O stretch amide-I at 1680 cm^{-1}, and N−H bend amide-II bands observed at 1550 and 1450 cm^{-1} are in line with this interpretation. The N−H stretch bands at 3050 and 3070 cm^{-1} (Figure 3b) signal the formation of a tight network of backbone−backbone interactions.

Lys2CP8 Association into Nanotubes. Light scattering and spectroscopy revealed that Lys2CP8 assembles into aggregates with a $β$-sheet rich secondary structure as encoded in the molecular design. To establish whether Lys2CP8 also adopts the desired nanotube morphology at high and low pH, cryogenic transmission electron microscopy (cryo-TEM) experiments were conducted on 5 mM Lys2CP8 solutions in 100 mM NaCl at pH 3 and 11. As expected, elongated structures were observed at both pH values (Figure 4). The impact of lysine side chain protonation on the aggregates is evident from a direct comparison between the micrographs taken at pH 3 (Figure 4a) and pH 11 (Figure 4b). Smaller
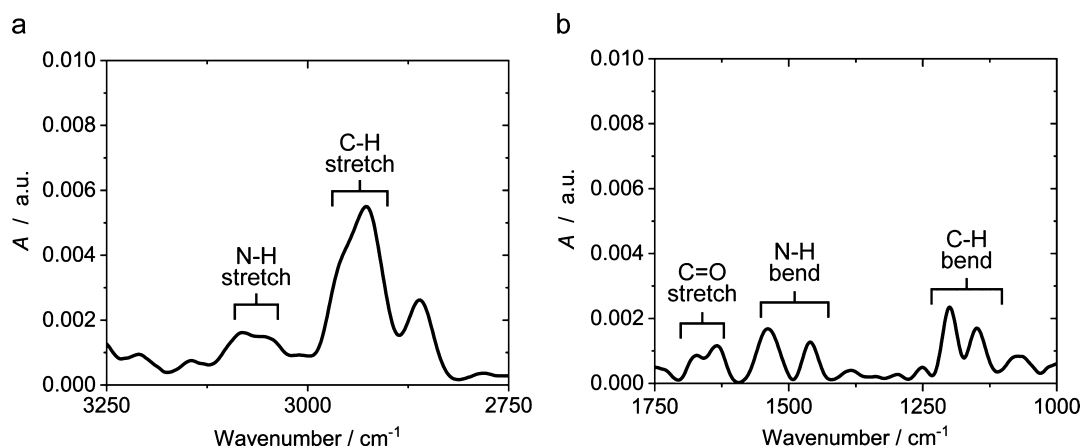
Figure 3. FTIR spectra of Lys2CP8 in solid state displaying the (a) N−H and C−H stretch vibrational regime and the (b) amide-I and amide-II bands in the N−H and C=O vibrational regime.
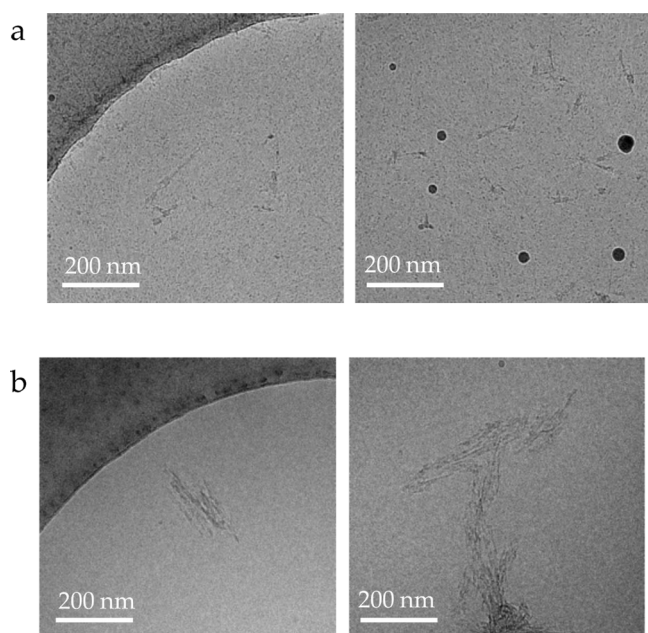

Figure 4. CryoTEM. Exemplary micrographs of 5 mM Lys2CP8 in 100 mM NaCl at (a) pH 3 and (b) pH 11. Dark spherical objects are crystalline ice particles.

tubular aggregates are visible at low pH values. Large bundled stacks are observed under basic conditions when the solution pH exceeds the pK_{aLys}. These electron micrographs shed further light on the origin of the observed increase in R_h as determined by light scattering upon increasing concentration at pH 11. The larger dimensions are in large part due to an increased tendency of the nanotube-forming peptides to also associate laterally at low degrees of ionization and high peptide concentrations.

Interaction of Lys2CP8 Nanotubes with Ice. The Lys2CP8 peptides assemble as designed in a pH-dependent manner into nanotubes guided by the formation of intermolecular β-sheets. This configuration projects the incorporated TaT ice-binding motif outward, so that it is accessible to mediate the interaction of the nanotubes with ice. To study whether this enables the self-assembled cyclic peptide nanotubes to inhibit ice recrystallization, IRRINA assays of ice recrystallization inhibition (IRI) activity were performed at

Lys2CP8 concentrations spanning ~2 orders of magnitude from $0.1 \leq [\text{Lys2CP8}] \leq 15$ mM under acidic conditions and from $0.1 \leq [\text{Lys2CP8}] \leq 10$ mM under basic conditions (Figure 5). Peptide concentrations exceeding 10 mM were inaccessible at pH 11 due to pronounced aggregation and precipitation (visible to the naked eye).

Figure 5 displays illustrative micrographs collected at 20 min intervals during a 60 min IRI assay at pH 3 (top panel) and pH 11 (bottom panel). Interestingly, the average size of the ice crystals increases markedly while their total number significantly reduces in all pH 11 Lys2CP8 samples. Apparently, none of the investigated CP concentrations is sufficiently high to prevent recrystallization under basic conditions. By contrast, differences in the ice crystal population are much smaller at pH 3. Both the increase in ice crystal size and the reduction in ice crystal number density are less pronounced for >2.5 mM Lys2CP8 concentrations under acidic conditions. Oval and rodlike ice crystals are clearly visible in the time lapse images taken at pH 3, wheras ice crystals grown at pH 11 are mostly circular. These notable deviations in ice crystal morphology and hampered ice crystal growth are both tell-tale signs of the ability of Lys2CP8 at pH 3 to interact with ice and more specifically, of its ability to inhibit ice recrystallization. To quantify the inhibition efficiency of Lys2CP8, the temporal evolution of the dimensions of the ice crystals in the suspensions (represented by $\langle R \rangle^3$) was determined for all peptide concentrations at pH 3 and 11 (Figures S4, S5).[7,44] These results were analyzed within the LSW framework,[8] which allows extraction of the ice crystal growth rates (k) from the time-evolution of $\langle R \rangle^3$ using

$$\langle R \rangle_t^3 = \langle R \rangle_0^3 + k \cdot t \tag{1}$$

These rates are subsequently rescaled to an ice crystal volume fraction of zero φ^0 and normalized by the ice growth rate of the solvent (k and k_0) without ice recrystallization inhibitor to obtain k_0 (Figure 6, Table S2), which can be used for a direct comparison of inhibitor effectivity irrespective of the details of the IRRINA assay (see Supporting Information for more details on the procedure).

Quantification of the IRI results reveals that the recrystallization rates k_0 are virtually concentration-independent at pH 11 ($k_0 \sim 1.87~\mu m^3~min^{-1} \pm 0.22~\mu m^3~min^{-1}$) and, moreover, comparable to the recrystallization rate of the reference sample without peptides (Figure 6) for which we determined $k_0 = 1.83$
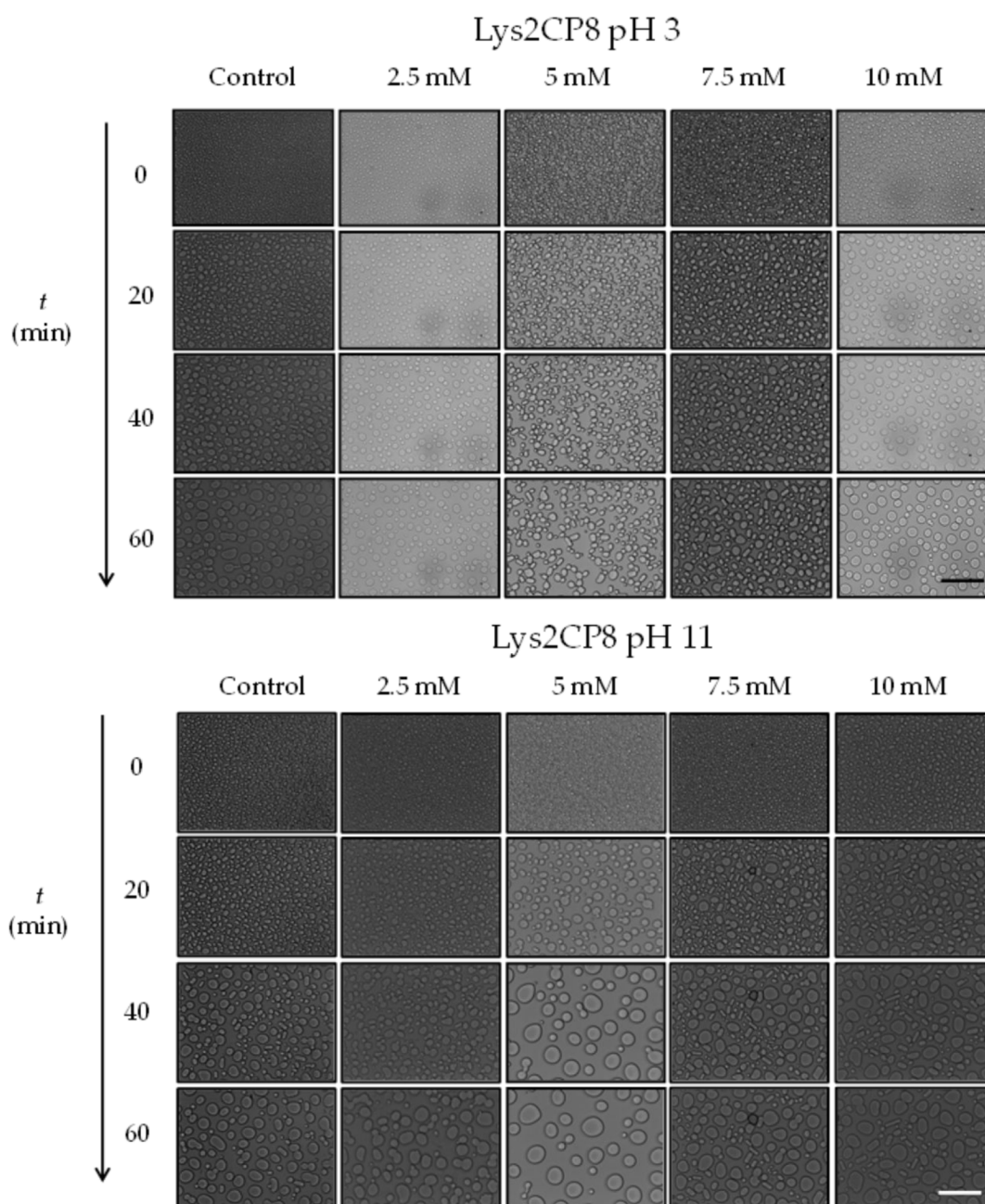
Figure 5. Optical microscopy. Micrographs obtained using transmission optical microscopy to assess IRI activity of the synthesized cyclic peptides at a set annealing temperature of −7 °C. Scale bars represent 100 μm.

μm^3 min^{-1} This suggests that the large aggregates observed under alkaline conditions are not IRI-active, possibly as the ice-binding sites are buried due to lateral aggregation of the one-dimensional aggregates into larger bundles. In stark contrast, at pH 3 we find a pronounced and nonmonotonic concentration-dependent IRI-activity for Lys2CP8 with 0.43 μm^3 min^{-1} ≤ k_0 ≤ 1.60 μm^3 min^{-1} (Figure 6). Surprisingly, [Lys2CP8] = 10 mM samples exhibited a larger $k_0 = 0.77$ μm^3 min^{-1} compared to samples at lower concentrations (2.5 ≤ [Lys2CP8] ≤ 7.5 mM). This minimum in k_0 at a Lys2CP8 monomer concentration of 5 mM means that IRI activity is higher for 2.5 ≤ [Lys2CP8] ≤ 7.5 mM than at [Lys2CP8] = 10 mM. This is unexpected since usually for natural AFPs and synthetic materials such as poly(vinyl)[45,46] the higher the concentration of ice recrystallization inhibitor in solution is, the lower the k

is. Tentatively, we propose that the reduced activity at pH 3 at concentrations above 7.5 mM is related to secondary aggregation at these high peptide concentrations. As observed by cryo-TEM at 5 mM at pH 11, we find bundled superstructures at pH 3 and 10 mM (Figure S6). We speculate that the TaT motif becomes (partially) buried within these aggregates, resulting in an apparent deactivation of the material. As an additional control experiment, we have also determined the ice crystal growth rates in the presence of the linear peptide Lys2LP8 (Figure S4c,d and Figure S5), which displays little IRI activity, supporting the conjecture that cyclization is necessary to generate IRI-active architectures.

A useful metric of IRI activity is the c_i which we determined for the IRI active material at pH 3, as is customary, using[8,46]
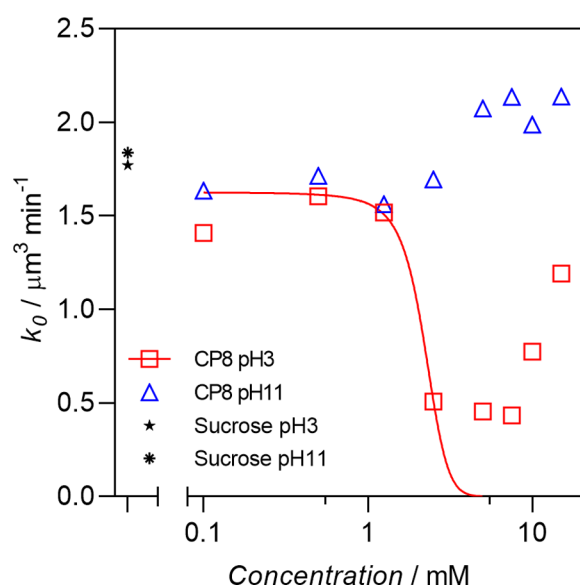
Figure 6. IRRINA assays of IRI activity. Ice crystal growth rates of Lys2CP8 samples rescaled to zero ice volume fraction, k_0, for Lys2CP8 as a function of concentration ($0.1 \leq c = [\text{Lys2CP8}] \leq 15$ mM) at (squares) pH 3 and (triangles) pH 11. A fit with eq 2 to the pH 3 data up to 5 mM is represented by the solid line. This yields an inhibitory LysCP8 concentration c_i = 2.2 mM.[8]

$$k_{(c)} = k_0 - \frac{k_0}{1 + e^{\left(\frac{c_i - c}{s}\right)}} \tag{2}$$

taking into account Lys2CP8 concentrations up to 5 mM only in view of the unusual nonmonotonic concentration dependence of the growth inhibition. This gives c_i = 2.2 mM for Lys2CP8 at pH 3. This IRI-activity is comparable to the IRI activity of various synthetic ice growth inhibitors,[45,46] such as poly(vinyl alcohol) and poly(vinyl alcohol)-based polymer micelles, with c_i = 0.38 mM[45,47] (linear PVA) and c_i = 0.33 mM[45] (PVA-micelles). It is lower than that of naturally occurring AFPs, which typically display a c_i in the submicromolar range.[46] For example, reported c_i's of ice-binding proteins from the beetle Dendroides canadensis (DAFP-1), ocean pout (QAE), and Antarctic Notothenioid fishes (AFGP$_{1-5}$) are 2.1 μM, 5.9 μM, and 0.91 nM, respectively.[7] Tentatively, we propose that this modest IRI activity may be due to the rather large aggregate size. Potent IRI active compounds, such as *Tm*AFPs, are much smaller than the aggregates formed by Lys2CP8. While the nanotubes are at least tens of nanometers long at pH 11, tmAFP is a rodlike object of 1.3 nm × 2.5 nm.[48] The IRI-activity of Lys2CP8 may thus be enhanced if the size and bundling of the CP aggregates could be fine-tuned. In line with previous work and hypotheses reported by others, we speculate that a large ice-binding surface (such as present here due to CP assembly and bundling) may promote ice nucleation and compromise IRI-activity.[49] This idea is supported by theoretical considerations[48] and the relatively large size of the ice-binding surface of ice-nucleating proteins (INPs) present in the cellular membrane of certain Gram-positive bacteria. These INPs display an IBS of over 50 repetitive units exposing a TXT motif to the environment.[50,51] To test this conjecture, it would be interesting to add a chain stopper to limit supramolecular aggregation or cross-link the cyclic peptides into tubes of discrete sizes.

CONCLUSIONS

In conclusion, we synthesized a cyclic octapeptide bearing the TaT motif targeting ice binding upon formation of self-assembled aggregates with solvent-accessible TaT regions resembling the structures of *Tm*AFP and *sbw*AFP. Lys2CP8 formed nanotubes in solution through backbone−backbone hydrogen bonding of the cyclic peptides, which generates a network of intermolecular antiparallel β-sheets as determined by CD and FTIR spectroscopy. The solution assembly, aggregate size, and shape of Lys2CP8 were studied by light scattering and cryo-TEM. Smaller superstructures were detected by light scattering at pH 3 than at pH 11, which is thought to be caused by electrostatic repulsion due to the high degree of ionization at pH 3, which is far below the $pK_{aLys} \sim$ 10.5 of the lysines incorporated within the cyclic peptides. Cryo-TEM confirmed the pH-dependent assembly revealed by light scattering and demonstrated that Lys2CP8 tends to cluster into bundles at pH 11. The ability of Lys2CP8 nanotubes to inhibit ice recrystallization was evaluated by the well-established IRRINA assay of IRI activity. Interestingly, the bundles observed at pH 11 were found to be IRI-inactive, whereas a concentration-dependent IRI activity was observed at pH = 3. Strikingly, an unusual re-entrant inactivity was observed at concentrations higher than 5 mM. We propose this to be related to the accessibility of the ice-binding sites, which may be (partially) buried and unable to interact with ice upon aggregation of individual nanotubes into bundles.

This proof-of-concept demonstration of ice recrystallization inhibition by a self-assembling cyclic peptide establishes the foundation for future work on ice-binders based on nanotube forming peptides. It would be of great interest to perform detailed structure−activity relationship studies on Lys2CP8 libraries in more detail, for example, to determine whether alignment of the TaT regions is a prerequisite for IRI activity. If these ice-binding sequences align to form long, regular arrays of threonines on the surface of the nanotubes, does this happen before or upon contact with ice? Lys2CP8 was shown to be inactive under physiological conditions and could therefore not be used for cryopreservation and other biomedical applications. Such applications warrant further development of analogues that display ice binding under physiological conditions. Another topic of interest would be to develop routes to control the length and lateral aggregation of the nanotubes, so as to rigorously establish whether the dimensions of either the ice-binding site, the ice-binder, or both impact IRI activity and ice nucleation.

ASSOCIATED CONTENT

ⓢ Supporting Information

The Supporting Information is available free of charge at https://pubs.acs.org/doi/10.1021/acs.biomac.1c01267.

> Figure S1, synthesis route of Lys2CP8; Figure S2, LC-MS data; Figure S3, ^{1}H NMR; Figure S4, IRRINA assays; Figure S5, optical microscopy; Table S1, expected m/z for Lys2CP8; Table S2, summary of obtained values; Figure S6: cryo-TEM of 10 mM Lys2CP8 at pH 3 (PDF)

AUTHOR INFORMATION

Corresponding Author

Ilja K. Voets − *Laboratory of Self-Organizing Soft Matter, Department of Chemical Engineering and Chemistry,*

Eindhoven University of Technology, 5600 MB Eindhoven, The Netherlands; Institute for Complex Molecular Systems, Department of Chemical Engineering and Chemistry, Eindhoven University of Technology, 5600 MB Eindhoven, The Netherlands; ⓘ orcid.org/0000-0003-3543-4821; Email: i.voets@tue.nl

Authors

Romà Surís-Valls − *Laboratory of Self-Organizing Soft Matter, Department of Chemical Engineering and Chemistry, Eindhoven University of Technology, 5600 MB Eindhoven, The Netherlands; Institute for Complex Molecular Systems, Department of Chemical Engineering and Chemistry and Laboratory of Chemical Biology, Department of Chemical Engineering and Chemistry, Eindhoven University of Technology, 5600 MB Eindhoven, The Netherlands*

Tim P. Hogervorst − *Laboratory of Self-Organizing Soft Matter, Department of Chemical Engineering and Chemistry, Eindhoven University of Technology, 5600 MB Eindhoven, The Netherlands; Institute for Complex Molecular Systems, Department of Chemical Engineering and Chemistry, Eindhoven University of Technology, 5600 MB Eindhoven, The Netherlands;* ⓘ orcid.org/0000-0002-4686-6251

Sandra M. C. Schoenmakers − *Institute for Complex Molecular Systems, Department of Chemical Engineering and Chemistry, Eindhoven University of Technology, 5600 MB Eindhoven, The Netherlands*

Marco M. R. M. Hendrix − *Laboratory of Self-Organizing Soft Matter, Department of Chemical Engineering and Chemistry, Eindhoven University of Technology, 5600 MB Eindhoven, The Netherlands; Institute for Complex Molecular Systems, Department of Chemical Engineering and Chemistry, Eindhoven University of Technology, 5600 MB Eindhoven, The Netherlands*

Lech Milroy − *Laboratory of Chemical Biology, Department of Chemical Engineering and Chemistry, Eindhoven University of Technology, 5600 MB Eindhoven, The Netherlands;* ⓘ orcid.org/0000-0003-4601-0936

Complete contact information is available at:
https://pubs.acs.org/10.1021/acs.biomac.1c01267

Author Contributions

I.K.V. conceived the project, I.K.V. and R.S.V. designed the experiments. R.S.V. and S.M.C.S. performed the experiments for Lys2CP8, and M.M.C.H. and T.P.H. performed the experiments for Lys2LP8. R.S.V., L.M., T.P.H., and I.K.V. analyzed the data. R.S.V. and I.K.V. wrote the manuscript with contributions from all authors.

Notes

The authors declare no competing financial interest.

REFERENCES

(1) Davies, P. L. Ice-Binding Proteins: A Remarkable Diversity of Structures for Stopping and Starting Ice Growth. *Trends Biochem. Sci.* **2014**, *39* (11), 548−555.

(2) Voets, I. K. From Ice-Binding Proteins to Bio-Inspired Antifreeze Materials. *Soft Matter* **2017**, *13* (28), 4808−4823.

(3) Cziko, P. A.; DeVries, A. L.; Evans, C. W.; Cheng, C.-H. C. Antifreeze Protein-Induced Superheating of Ice inside Antarctic Notothenioid Fishes Inhibits Melting during Summer Warming. *Proc. Natl. Acad. Sci. U. S. A.* **2014**, *111* (40), 14583−14588.

(4) Bayer-Giraldi, M.; Sazaki, G.; Nagashima, K.; Kipfstuhl, S.; Vorontsov, D. A.; Furukawa, Y. Growth Suppression of Ice Crystal Basal Face in the Presence of a Moderate Ice-Binding Protein Does Not Confer Hyperactivity. *Proc. Natl. Acad. Sci. U. S. A.* **2018**, *115* (29), 7479−7484.

(5) Pandey, R.; Usui, K.; Livingstone, R. A.; Fischer, S. A.; Pfaendtner, J.; Backus, E. H. G.; Nagata, Y.; Fröhlich-Nowoisky, J.; Schmüser, L.; Mauri, S.; Scheel, J. F.; Knopf, D. A.; Pöschl, U.; Bonn, M.; Weidner, T. Ice-Nucleating Bacteria Control the Order and Dynamics of Interfacial Water. *Sci. Adv.* **2016**, *2* (4), No. e1501630.

(6) Bredow, M.; Walker, V. K. Ice-Binding Proteins in Plants. *Front. Plant Sci.* **2017**, *8* (2153), 1−15.

(7) Olijve, L. L. C.; Meister, K.; DeVries, A. L.; Duman, J. G.; Guo, S.; Bakker, H. J.; Voets, I. K. Blocking Rapid Ice Crystal Growth through Nonbasal Plane Adsorption of Antifreeze Proteins. *Proc. Natl. Acad. Sci. U. S. A.* **2016**, *113* (14), 3740−3745.

(8) Budke, C.; Heggemann, C.; Koch, M.; Sewald, N.; Koop, T. Ice Recrystallization Kinetics in the Presence of Synthetic Antifreeze Glycoprotein Analogues Using the Framework of LSW Theory. *J. Phys. Chem. B* **2009**, *113* (9), 2865−2873.

(9) Guo, S.; Stevens, C. A.; Vance, T. D. R.; Olijve, L. L. C.; Graham, L. A.; Campbell, R. L.; Yazdi, S. R.; Escobedo, C.; Bar-Dolev, M.; Yashunsky, V.; Braslavsky, I.; Langelaan, D. N.; Smith, S. P.; Allingham, J. S.; Voets, I. K.; Davies, P. L. Structure of a 1.5-MDa Adhesin That Binds Its Antarctic Bacterium to Diatoms and Ice. *Sci. Adv.* **2017**, *3* (8), No. e1701440.

(10) Abraham, S.; Keillor, K.; Capicciotti, C. J.; Perley-Robertson, G. E.; Keillor, J. W.; Ben, R. N. Quantitative Analysis of the Efficacy and Potency of Novel Small Molecule Ice Recrystallization Inhibitors. *Cryst. Growth Des.* **2015**, *15* (10), 5034−5039.

(11) Surís-Valls, R.; Voets, I. K. Peptidic Antifreeze Materials: Prospects and Challenges. *Int. J. Mol. Sci.* **2019**, *20* (20), 5149.

(12) Stevens, C. A.; Bachtiger, F.; Kong, X.-D.; Abriata, L. A.; Sosso, G. C.; Gibson, M. I.; Klok, H.-A. A Minimalistic Cyclic Ice-Binding Peptide from Phage Display. *Nat. Commun.* **2021**, *12* (1), 2675.

(13) Xue, B.; Zhao, L.; Qin, X.; Qin, M.; Lai, J.; Huang, W.; Lei, H.; Wang, J.; Wang, W.; Li, Y.; Cao, Y. Bioinspired Ice Growth Inhibitors Based on Self-Assembling Peptides. *ACS Macro Lett.* **2019**, *8* (10), 1383−1390.

(14) Biggs, C. I.; Stubbs, C.; Graham, B.; Fayter, A. E. R.; Hasan, M.; Gibson, M. I. Mimicking the Ice Recrystallization Activity of Biological Antifreezes. When Is a New Polymer "Active"? *Macromol. Biosci.* **2019**, *19* (7), 1900082.

(15) Graham, B.; Fayter, A. E. R.; Houston, J. E.; Evans, R. C.; Gibson, M. I. Facially Amphipathic Glycopolymers Inhibit Ice Recrystallization. *J. Am. Chem. Soc.* **2018**, *140* (17), 5682−5685.

(16) Garnham, C. P.; Campbell, R. L.; Davies, P. L. Anchored Clathrate Waters Bind Antifreeze Proteins to Ice. *Proc. Natl. Acad. Sci. U. S. A.* **2011**, *108* (18), 7363.

(17) Rodriguez-Vazquez, N.; Amorin, M.; Granja, J. R. Recent Advances in Controlling the Internal and External Properties of Self-Assembling Cyclic Peptide Nanotubes and Dimers. *Org. Biomol. Chem.* **2017**, *15* (21), 4490−4505.

(18) Castelletto, V.; Nutt, D. R.; Hamley, I. W.; Bucak, S.; Cenker, C.; Olsson, U. Structure of Single-Wall Peptide Nanotubes: In Situ Flow Aligning X-Ray Diffraction. *Chem. Commun.* **2010**, *46* (34), 6270−6272.

(19) Ashkenasy, N.; Horne, W. S.; Ghadiri, M. R. Design of Self-Assembling Peptide Nanotubes with Delocalized Electronic States. *Small* **2006**, *2* (1), 99−102.

(20) Hendricks, M. P.; Sato, K.; Palmer, L. C.; Stupp, S. I. Supramolecular Assembly of Peptide Amphiphiles. *Acc. Chem. Res.* **2017**, *50* (10), 2440−2448.

(21) Hua, W.; Wang, Y.; Guo, C.-Y.; Wang, J.; Li, S.; Guo, L. Ice Recrystallization Inhibition Activity of Protein Mimetic Peptoids. *J. Inorg. Organomet. Polym. Mater.* **2021**, *31*, 203−208.

(22) Huang, M. L.; Ehre, D.; Jiang, Q.; Hu, C.; Kirshenbaum, K.; Ward, M. D. Biomimetic Peptoid Oligomers as Dual-Action Antifreeze Agents. *Proc. Natl. Acad. Sci. U. S. A.* **2012**, *109* (49), 19922−19927.

(23) Hartgerink, J. D.; Granja, J. R.; Milligan, R. A.; Ghadiri, M. R. Self-Assembling Peptide Nanotubes. *J. Am. Chem. Soc.* **1996**, *118* (1), 43−50.

(24) Danial, M.; My-Nhi Tran, C.; Young, P. G.; Perrier, S.; Jolliffe, K. A. Janus Cyclic Peptide-Polymer Nanotubes. *Nat. Commun.* **2013**, *4* (1), 2780.

(25) Ghadiri, M. R.; Granja, J. R.; Milligan, R. A.; McRee, D. E.; Khazanovich, N. Self-Assembling Organic Nanotubes Based on a Cyclic Peptide Architecture. *Nature* **1993**, *366* (6453), 324−327.

(26) Qin, S.-Y.; Xu, X.-D.; Chen, C.-S.; Chen, J.-X.; Li, Z.-Y.; Zhuo, R.-X.; Zhang, X.-Z. Supramolecular Architectures Self-Assembled from Asymmetrical Hetero Cyclopeptides. *Macromol. Rapid Commun.* **2011**, *32* (9−10), 758−764.

(27) Rho, J. Y.; Cox, H.; Mansfield, E. D. H.; Ellacott, S. H.; Peltier, R.; Brendel, J. C.; Hartlieb, M.; Waigh, T. A.; Perrier, S. Dual Self-Assembly of Supramolecular Peptide Nanotubes to Provide Stabilisation in Water. *Nat. Commun.* **2019**, *10* (1), 4708.

(28) Sreerama, N.; Woody, R. W. Estimation of Protein Secondary Structure from Circular Dichroism Spectra: Comparison of CONTIN, SELCON, and CDSSTR Methods with an Expanded Reference Set. *Anal. Biochem.* **2000**, *287* (2), 252−260.

(29) Whitmore, L.; Wallace, B. A. DICHROWEB, an Online Server for Protein Secondary Structure Analyses from Circular Dichroism Spectroscopic Data. *Nucleic Acids Res.* **2004**, *32*, W668−W673.

(30) Hartlieb, M.; Catrouillet, S.; Kuroki, A.; Sanchez-Cano, C.; Peltier, R.; Perrier, S. Stimuli-Responsive Membrane Activity of Cyclic-Peptide-Polymer Conjugates. *Chem. Sci.* **2019**, *10* (21), 5476−5483.

(31) Burade, S. S.; Saha, T.; Bhuma, N.; Kumbhar, N.; Kotmale, A.; Rajamohanan, P. R.; Gonnade, R. G.; Talukdar, P.; Dhavale, D. D. Self-Assembly of Fluorinated Sugar Amino Acid Derived α,γ-Cyclic Peptides into Transmembrane Anion Transport. *Org. Lett.* **2017**, *19* (21), 5948−5951.

(32) Ghadiri, M. R.; Granja, J. R.; Buehler, L. K. Artificial Transmembrane Ion Channels from Self-Assembling Peptide Nanotubes. *Nature* **1994**, *369* (6478), 301−304.

(33) Chakraborty, S.; Jana, B. Molecular Insight into the Adsorption of Spruce Budworm Antifreeze Protein to an Ice Surface: A Clathrate-Mediated Recognition Mechanism. *Langmuir* **2017**, *33* (28), 7202−7214.

(34) Doucet, D.; Tyshenko, M. G.; Kuiper, M. J.; Graether, S. P.; Sykes, B. D.; Daugulis, A. J.; Davies, P. L.; Walker, V. K. Structure-Function Relationships in Spruce Budworm Antifreeze Protein Revealed by Isoform Diversity. *Eur. J. Biochem.* **2000**, *267* (19), 6082−6088.

(35) Brotzakis, Z. F.; Gehre, M.; Voets, I. K.; Bolhuis, P. G. Stability and Growth Mechanism of Self-Assembling Putative Anti-Freeze Cyclic Peptides. *Phys. Chem. Chem. Phys.* **2017**, *19*, 19032−19042.

(36) Behrendt, R.; White, P.; Offer, J. Advances in Fmoc Solid-Phase Peptide Synthesis. *J. Pept. Sci.* **2016**, *22* (1), 4−27.

(37) Dourtoglou, V.; Ziegler, J.-C.; Gross, B. L'hexafluorophosphate de O-Benzotriazolyl-N,N-Tetramethyluronium: Un Reactif de Couplage Peptidique Nouveau et Efficace. *Tetrahedron Lett.* **1978**, *19* (15), 1269−1272.

(38) Hood, C. A.; Fuentes, G.; Patel, H.; Page, K.; Menakuru, M.; Park, J. H. Fast Conventional Fmoc Solid-Phase Peptide Synthesis with HCTU. *J. Pept. Sci.* **2008**, *14* (1), 97−101.

(39) Coste, J.; Le-Nguyen, D.; Castro, B. PyBOP®: A New Peptide Coupling Reagent Devoid of Toxic by-Product. *Tetrahedron Lett.* **1990**, *31* (2), 205−208.

(40) Raw, S. A. An Improved Process for the Synthesis of DMTMM-Based Coupling Reagents. *Tetrahedron Lett.* **2009**, *50* (8), 946−948.

(41) Vijayaraj, R.; Sundar Raman, S.; Mahesh Kumar, R.; Subramanian, V. Studies on the Structure and Stability of Cyclic Peptide Based Nanotubes Using Oligomeric Approach: A Computational Chemistry Investigation. *J. Phys. Chem. B* **2010**, *114* (49), 16574−16583.

(42) Naik, V. M.; Krimm, S. Vibrational Analysis of the Structure of Gramicidin A. II. Vibrational Spectra. *Biophys. J.* **1986**, *49* (6), 1147−1154.

(43) Chen, J.; Li, Q.; Wu, P.; Liu, J.; Wang, D.; Yuan, X.; Zheng, R.; Sun, R.; Li, L. Cyclic γ-Peptides With Transmembrane Water Channel Properties. *Front. Chem.* **2020**, *8*, 368.

(44) Suris-Valls, R.; Voets, I. K. The Impact of Salts on the Ice Recrystallization Inhibition Activity of Antifreeze (Glyco)Proteins. *Biomolecules* **2019**, *9* (8), 347.

(45) Sproncken, C. C. M.; Surís-Valls, R.; Cingil, H. E.; Detrembleur, C.; Voets, I. K. Complex Coacervate Core Micelles Containing Poly(Vinyl Alcohol) Inhibit Ice Recrystallization. *Macromol. Rapid Commun.* **2018**, *39* (17), 1700814.

(46) Budke, C.; Dreyer, A.; Jaeger, J.; Gimpel, K.; Berkemeier, T.; Bonin, A. S.; Nagel, L.; Plattner, C.; DeVries, A. L.; Sewald, N.; Koop, T. Quantitative Efficacy Classification of Ice Recrystallization Inhibition Agents. *Cryst. Growth Des.* **2014**, *14* (9), 4285−4294.

(47) Olijve, L. L. C.; Hendrix, M. M. R. M.; Voets, I. K. Influence of Polymer Chain Architecture of Poly(Vinyl Alcohol) on the Inhibition of Ice Recrystallization. *Macromol. Chem. Phys.* **2016**, *217* (8), 951−958.

(48) Ling, M. L.; Wex, H.; Grawe, S.; Jakobsson, J.; Löndahl, J.; Hartmann, S.; Finster, K.; Boesen, T.; Santl-Temkiv, T. Effects of Ice Nucleation Protein Repeat Number and Oligomerization Level on Ice Nucleation Activity. *J. Geophys. Res. Atmos.* **2018**, *123* (3), 1802−1810.

(49) Mueller, G. M.; Wolber, P. K.; Warren, G. J. Clustering of Ice Nucleation Protein Correlates with Ice Nucleation Activity. *Cryobiology* **1990**, *27* (4), 416−422.

(50) Graether, S. P.; Jia, Z. C. Modeling Pseudomonas Syringae Ice-Nucleation Protein as a Beta-Helical Protein. *Biophys. J.* **2001**, *80* (3), 1169−1173.

(51) Kassmannhuber, J.; Rauscher, M.; Schöner, L.; Witte, A.; Lubitz, W. Functional Display of Ice Nucleation Protein InaZ on the Surface of Bacterial Ghosts. *Bioengineered* **2017**, *8* (5), 488−500.